◆ Human Brain Mapping 36:2027–2038 (2015) ◆

Default-Mode Network Functional Connectivity is Closely Related to Metabolic Activity

Susanne Passow,[1,2]* Karsten Specht,[1,3] Tom Christian Adamsen,[4,5] Martin Biermann,[4,6] Njål Brekke,[4,7] Alexander Richard Craven,[1,2] Lars Ersland,[2,3] Renate Grüner,[2,4,8] Nina Kleven-Madsen,[4] Ole-Heine Kvernenes,[4] Thomas Schwarzlmüller,[4,6] Rasmus Aamand Olesen,[9] and Kenneth Hugdahl[1,2,4,10]

[1]*Department of Biological and Medical Psychology, University of Bergen, Bergen, Norway*
[2]*NORMENT Center of Excellence, University of Oslo, Norway*
[3]*Department of Clinical Engineering, Haukeland University Hospital, Bergen, Norway*
[4]*Department of Radiology, Haukeland University Hospital, Bergen, Norway*
[5]*Department of Chemistry, University of Bergen, Bergen, Norway*
[6]*Department of Clinical Medicine, University of Bergen, Bergen, Norway*
[7]*Department of Oncology and Medical Physics, Haukeland University Hospital, Bergen, Norway*
[8]*Department of Physics and Technology, University of Bergen, Bergen, Norway*
[9]*Center of Functionally Integrative Neuroscience and MINDLab, Aarhus University, Aarhus, Denmark*
[10]*Division of Psychiatry, Haukeland University Hospital, Bergen, Norway*

Abstract: Over the last decade, the brain's default-mode network (DMN) and its function has attracted a lot of attention in the field of neuroscience. However, the exact underlying mechanisms of DMN functional connectivity, or more specifically, the blood-oxygen level-dependent (BOLD) signal, are still incompletely understood. In the present study, we combined 2-deoxy-2-[^{18}F]fluoroglucose positron emission tomography (FDG-PET), proton magnetic resonance spectroscopy (^{1}H-MRS), and resting-state functional magnetic resonance imaging (rs-fMRI) to investigate more directly the association between local glucose consumption, local glutamatergic neurotransmission and DMN functional connectivity during rest. The results of the correlation analyzes using the dorsal posterior cingulate cortex (dPCC) as seed region showed spatial similarities between fluctuations in FDG-uptake and fluctuations in BOLD signal. More specifically, in both modalities the same DMN areas in the inferior parietal lobe, angular gyrus, precuneus, middle, and medial frontal gyrus were positively correlated with the dPCC. Furthermore, we could demonstrate that local glucose consumption in the medial frontal gyrus, PCC and left angular gyrus was associated with functional connectivity within the DMN. We did not, however, find a relationship between glutamatergic neurotransmission and functional connectivity. In line with very recent findings, our results lend further support for a close association between local metabolic activity and functional connectivity and provide further insights towards a better understanding of the underlying mechanism of the BOLD signal. *Hum Brain Mapp 36:2027–2038, 2015.*

Additional Supporting Information may be found in the online version of this article.

Susanne Passow and Karsten Specht contributed equally well to this work.

Contract grant sponsor: European Research Council; Contract grant number: ERC AG #249516 (to K.H.); Contract grant sponsor: Research Council of Norway; Contract grant numbers: RCN # 196076; #222373 (to K.H.)

*Correspondence to: Susanne Passow; Department of Biological and Medical Psychology, University of Bergen, Jonas Lies vei 91, 5009 Bergen, Norway. E-mail: susanne.passow@psybp.uib.no

Received for publication 2 December 2014; Revised 14 January 2015; Accepted 20 January 2015.

DOI: 10.1002/hbm.22753

Published online 3 February 2015 in Wiley Online Library (wileyonlinelibrary.com).

Key words: FDG-PET; resting-state fMRI; ^{1}H-MR spectroscopy; default-mode network; resting-state functional connectivity

INTRODUCTION

Basic and cognitive neuroscience has taken great advantage of functional magnetic resonance imaging (fMRI) as a noninvasive method to further advance our understanding of brain function. fMRI research has shown that brain activity in the absence of any explicit task is characterized by low-frequency (<0.1 Hz) fluctuations in blood oxygen level-dependent (BOLD) signal that are synchronized between brain regions [e.g., Biswal et al., 1995; Fox and Raichle, 2007; Greicius et al., 2003]. This so-called resting-state functional connectivity within and across brain networks is consistently observed across subjects and even across species [e.g., Damoiseaux et al., 2006; Vincent et al., 2007]. Of specific interest for this study is the default-mode network [DMN; Raichle et al., 2001]. In contrast to other resting-state networks (RSNs), the DMN is functionally defined as being more active during rest than during a wide range of attention-demanding tasks. Anatomically the DMN consists of the posterior cingulate cortex (PCC)/precuneus, medial frontal, inferior parietal regions, and medial temporal lobe (van den Heuvel and Pol, 2010]. DMN functional connectivity is anticorrelated with functional connectivity of task-positive networks, that is, networks usually involved in attention-demanding tasks [Fox et al., 2005]. This reciprocal relationship is thought to function as a shift between two modes of information processing, one serving internal inner thoughts and one serving task-related attention. The task-dependent down-regulation of the DMN is a fundamental property of the human brain and has been suggested to play a pivotal role in the pathophysiology of mental disorders [see Whitfield-Gabrieli and Ford, 2012 for overview].

Resting-state functional connectivity research has advanced our understanding of brain function in healthy subjects and clinical disorders. However, its underlying neurophysiological and metabolic mechanisms are still not completely understood [e.g., Brookes et al., 2011, Raichle, 2010, Wehrl et al., 2013, Wu et al., 2009]. Measuring more directly neuronal activity using magnetoencephalography (MEG), Brookes et al., (2011) have shown a significant similarity between RSNs derived from MEG and fMRI supporting a neuronal basis of these hemodynamic networks. Further, the BOLD signal is triggered by the metabolic demands of increased brain activation. During neuronal activity, increases in blood flow are paralleled by increases in local glucose and oxygen consumption. About 80–90% of the total cortical glucose consumption is used for supplying energy to excitatory glutamatergic neurotransmission [e.g., Bonvento et al., 2002; Lauritzen, 2005; Logothetis and Wandell, 2004; Shulman et al., 2001]. Thus, the BOLD signal is based on interactions between cerebral metabolic rate of oxygen ($CMRO_2$) and glucose (CMRGlc), cerebral blood flow, and cerebral blood volume [e.g., Buxton et al., 1998; Heeger and Ress, 2002; Raichle, 1987, 2010] that are in turn related to glutamatergic neurotransmission and there is a considerable interest in elucidating this complex interplay.

Studies combining proton magnetic resonance spectroscopy (^{1}H-MRS) and fMRI show that local resting-state glutamate concentration predicts the strength of BOLD response during rest [Enzi et al., 2012] and cognitive tasks [Falkenberg et al., 2012; Hu et al., 2013]. To explore the link between local oxygen and glucose consumption, recent neuroimaging studies investigated whether $CMRO_2$ [Wu et al., 2009] and CMRGlc [Riedl et al., 2014; Tomasi et al., 2013; Wehrl et al., 2013], respectively, are related to fluctuations in BOLD response. Wu et al., (2009) examined the association between BOLD, perfusion, and $CMRO_2$. $CMRO_2$ was calculated from simultaneously acquired BOLD and perfusion signals. This study revealed synchronized spontaneous fluctuations during resting state on both hemodynamic (BOLD and perfusion) and metabolic ($CMRO_2$) level suggesting that spontaneous fMRI signal fluctuations likely derive from dynamic changes in cerebral metabolism reflecting ongoing neuronal activity [Wu et al., 2009]. However, although $CMRO_2$ estimations have been shown to overlap with positron emission tomography (PET)-derived measures [Ai-Ling et al., 2008], $CMRO_2$ is only based on a biophysical model derived from indirect hemodynamic signals.

To investigate the link between direct measures of local glucose consumption and functional coupling within and across brain networks, recent multimodal studies combined 2-deoxy-2-[^{18}F]fluoroglucose (FDG)-PET with fMRI. For instance, Tomasi et al. (2013) separately acquired resting-state functional connectivity and FDG-PET data. They revealed that higher glucose metabolism was associated with proportionally larger BOLD signal amplitudes and that glucose demand increased nonlinearly with the degree of functional connectivity [Tomasi et al., 2013]. Riedl et al. (2014) provided first evidence for the state dependence (eyes open vs. eyes closed) of this relationship in a simultaneous setup using an integrated PET/MRI scanner. These authors showed that local glucose consumption in primary visual areas was coupled with functional connectivity within the visual network independent of brain state. In contrast, increased between-network coupling in visual and salience network was accompanied by

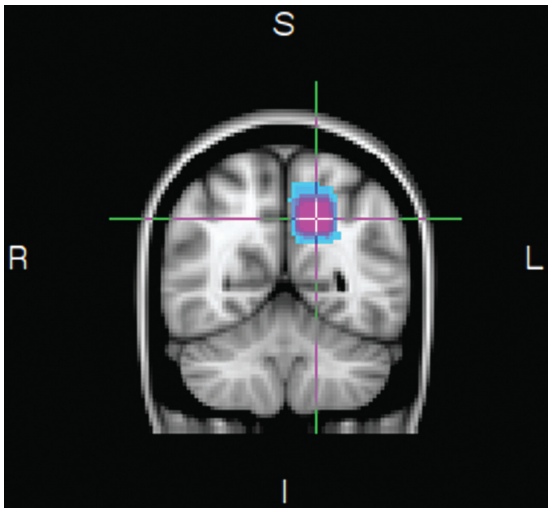

Figure 1.
Voxel placement for the ^{1}H-MRS measurement in the left precuneus across all participants. Note the figure is shown in radiological orientation (I = inferior, L = left, R = right, S = superior).

an increase in local glucose consumption only in eyes-opened and not in eyes-closed condition.

In summary, these studies provide evidence for a link between resting-state functional connectivity and metabolic activity and reflect the great potential of comparative recordings of FDG-PET and fMRI data for advancing our understanding of the BOLD signal and resting-state functional connectivity. To date, there is yet no study that investigates how fluctuations in BOLD signal during rest are associated with local glucose consumption on the one hand and local glutamatergic neurotransmission on the other. Thus, in the present study, we recorded rs-fMRI and FDG-PET data from the same participants and additionally applied ^{1}H-MRS to assess resting-state combined glutamate–glutamine (Glx) content in the precuneus, a key component of the DMN. Based on previous empirical evidence showing a direct link between metabolic activity and spontaneous BOLD fluctuations, we expected to find spatially overlapping functional connectivity maps in fMRI and PET data. To test these predictions, a new type of PET analysis was developed that rests on measuring the fluctuation in glucose uptake, which may indicate temporal and spatial variations in metabolic activity. It was aimed to test, whether the spatial characteristic of these variations corresponds to patterns that are by now only described for rs-fMRI. Furthermore, we expected that DMN within-network connectivity would be associated with local glucose consumption and glutamatergic neurotransmission.

MATERIALS AND METHODS

Participants

Eight healthy, right-handed male participants (mean age 53.1 ± 10.5) with no history of neurological or psychiatric conditions were included in the study. Standard MR-related exclusion criteria were applied. Participants were asked to fast the night before data acquisition. The session started early in the morning with the MRI data acquisition and was directly followed by the FDG-PET data recording (for more details see below). During both data acquisitions, participants were asked to lie still, keep their eyes open, relax, and to not think of anything in particular. All participants gave informed consent and were compensated (500 NOK) for participation. The study was approved by the Regional Committee for Medical and Health Research Ethics (REC West), according to the declaration of Helsinki.

MRI Data Acquisition

All imaging was performed on a GE Signa 3.0T Twin speed HDxt scanner (GE Healthcare, Waukesha, WI). The participants underwent an imaging protocol including structural imaging, rs-fMRI, and ^{1}H-MRS. Structural T1-weighted images were acquired using a three-dimensional (3D) fast spoiled gradient recalled sequence (TR = 7.9 ms; TE = 3.1 ms; 11° flip angle) measuring 180 sagittal slices (field of view, FOV = 256 × 256 mm^2; 256 × 256 scan matrix, slice thickness = 1mm). During rs-fMRI a set of 300 T2*-weighted volumes were collected with a two-dimensional (2D) gradient echo planar imaging sequence (TR = 1500 ms; TE = 30 ms, 90° flip angle; FOV = 220 × 220 mm^2; 64 × 64 scan matrix; slice thickness = 3 mm, gap = 1 mm, 25 slices per volume). Axial T2-weighted images were obtained before the ^{1}H-MRS to position the voxel. In vivo ^{1}H-MRS spectra were obtained from the left precuneus (see Fig. 1) using a single voxel PRESS sequence (TR = 1500 ms, TE = 35 ms, voxel size 20 × 20 × 20 mm, 128 averages). An iterative shimming procedure was used to ensure a line-width of less than 10 Hz and a water suppression level of at least 90%.

FDG-PET Data Acquisition

PET was performed on a Siemens Biograph 40 PET/CT system (Siemens Medical Solutions, Knoxville TN) using 180–200 MBq (4–6 mCi) 2-Deoxy-2-[^{18}F]fluoroglucose ([^{18}F]FDG) produced according to good manufacturing practice at the Centre for Nuclear Medicine/PET, Department of Radiology, Haukeland University Hospital. We measured blood pressure and fasting glucose levels (mean = 5.7 ± 0.9 mmol/L; 4.8–7.7 mmol/L) and prepared the participants with a venous catheter to receive radioactive agent injection. Before injection of the radioactive agent participants rested with eyes open on the scanner bench with their head properly adjusted and fixated by a vacuum-pillow to prevent major head movements during the extended scanning period. Images were acquired in 3D list-mode under resting conditions (eyes open) from 0 to 60 min postinjection. The raw acquisition data were reconstructed as 12 frames with frame duration of 300 s

using the ordered subset expectation maximization (OSEM) reconstruction algorithm [Tzoulis et al., 2013]. Parameters of the OSEM algorithm were: 4 iterations, 8 subsets, scatter correction using low dose CT, no filtering (all-pass), 336 × 336 matrix with 1.02 × 1.02 mm^2 pixel size, 3 mm slice thickness and 1.5 mm distance between slices. A 2× zoom factor were used in the reconstructions to limit the FOV from the scanner intrinsic FOV of 68.4 to 34.2 cm.

Resting-State fMRI Analysis

DICOM-images from the scanner were converted into 4D-NIfTI volumes and then processed with FSL v5.0 tools from the FMRIB Software library (www.fmrib.ox.ac.uk/fsl). The preprocessing consisted of brain extraction using BET [Smith, 2002], motion correction using MCFLIRT [Jenkinson et al., 2002], high-pass filtering with a frequency cut-off at 100 s, spatial smoothing at 5 mm full-width half-maximum, intensity normalization, and global rescale registration to the MNI 152 standard template with a resampling resolution of 2 mm.

DMN functional connectivity was investigated by first applying a temporal concatenation independent component analysis (ICA) approach (Beckmann et al., 2005). The preprocessed datasets of all participants were merged into one data set which was then concatenated and decomposed using MELODIC tool from FSL. Automatic dimensionality estimation identified 40 independent spatial components. Afterwards, the independent components (ICs) were visually inspected and compared with those reported in previously published rs-fMRI literature [Di et al., 2012; Rytty et al., 2013; Sala-Llonch et al., 2012; van den Heuvel and Pol, 2010]. The IC4 (see Fig. 4) was selected as it represents the anterior and dorsal parts of the DMN, that is, medial frontal gyrus (MdFG), PCC, right and left angular Gyrus (ANG). For each of the four nodes, the voxel with the highest *z*-statistics (see Table I) were identified and a spherical ROI with a radius of 8 mm around the peak voxel was created. Finally, individual mean time-series within these ROIs were obtained from the preprocessed rs-fMRI data. Temporal correlations between individual mean time series of each node, reflecting DMN within-network connectivity, were investigated by computing Pearson's correlation coefficients in MATLAB R2012b. Afterwards correlation coefficients were exported to IBM Statistical Package for the Social Science Statistics 19 for further joint data analysis (see below).

For a comparative analysis of the fMRI and PET data, each data set was subjected to a seed-based analysis of the DMN (see Fig. 2 and for a detailed description of the seed-based correlation analysis of the PET-data see below). The fMRI resting-sate data were preprocessed with standard SPM8 preprocessing, including realignment, unwarping—to correct for movement-by-distortion interactions—, normalization to the MNI template, and, finally, smoothing with a 12 mm Gaussian kernel.

TABLE I. Anatomical localization, MNI coordinates and maximum intensity of the peak voxel in each node of the default-mode network ($z > 4$; $k > 20$ voxel).

Region	MNI coordinates			*z*-value	Cluster size (#voxel)
	x	*y*	*z*		
Default-Mode Network					
Medial frontal gyrus	6	58	4	13.50	5011
Posterior cingulate	4	−52	24	14.40	2012
Left angular gyrus	−50	−64	30	7.23	568
Right angular gyrus	52	−64	36	6.89	366

The seed-based correlation analysis was performed by including local fluctuations in BOLD-signal from the dorsal PCC (dPCC). The MNI coordinate for the dPCC [0 −24 38] were taken from previous literature [Leech et al., 2011]. Leech et al., [2011] describe the dPCC as an area that is highly integrated with the DMN at rest, but appears also as a link between the DMN and cognitive control networks in demanding tasks. A spherical ROI around the MNI coordinate with a radius of 8 mm was created. The detrended and low-pass filtered (<0.1 Hz) BOLD fluctuations were included as regressor in a single-subject fMRI analysis. In addition, a high-pass filter of 128 s was applied. The individual beta-weights from this regression analysis were subjected to a second level analysis, which was a one-sample *t*-test across all eight participants, and age was included as an additional covariate. The results from this analysis were explored with a significance threshold of $P < 0.025$ [false-discovery rate (FDR)-corrected] and with at least 50 voxels per cluster, and post hoc increased to $P < 0.001$ (FDR-corrected) for a better separation of involved areas.

FDG-PET Data Analysis

As mentioned before, the FDG-PET list-mode data were reconstructed into twelve 5-min time-frames, and stored as DICOM images. As with the fMRI data, these images were converted into 4D-NifTi volumes. Slice thickness was manually adjusted to 1.5 mm to account for the overlapping slices. The 4D FDG-PET data were analyzed using statistical parametric mapping software (SPM8; www.fil.ion.ucl.ac.uk/spm) toolbox. First, the images were corrected for all head movements (realignment) that occurred during the 60 min of data acquisition. Second, the data were normalized into the MNI standard space. This was achieved by transforming an averaged PET image, created during the realignment procedure, into the MNI space, represented by a standard FDG-PET template. The estimated, nonlinear transformation was subsequently applied to all twelve time frames. Finally, the data were smoothed with a Gaussian kernel of 12 mm (FWHM).

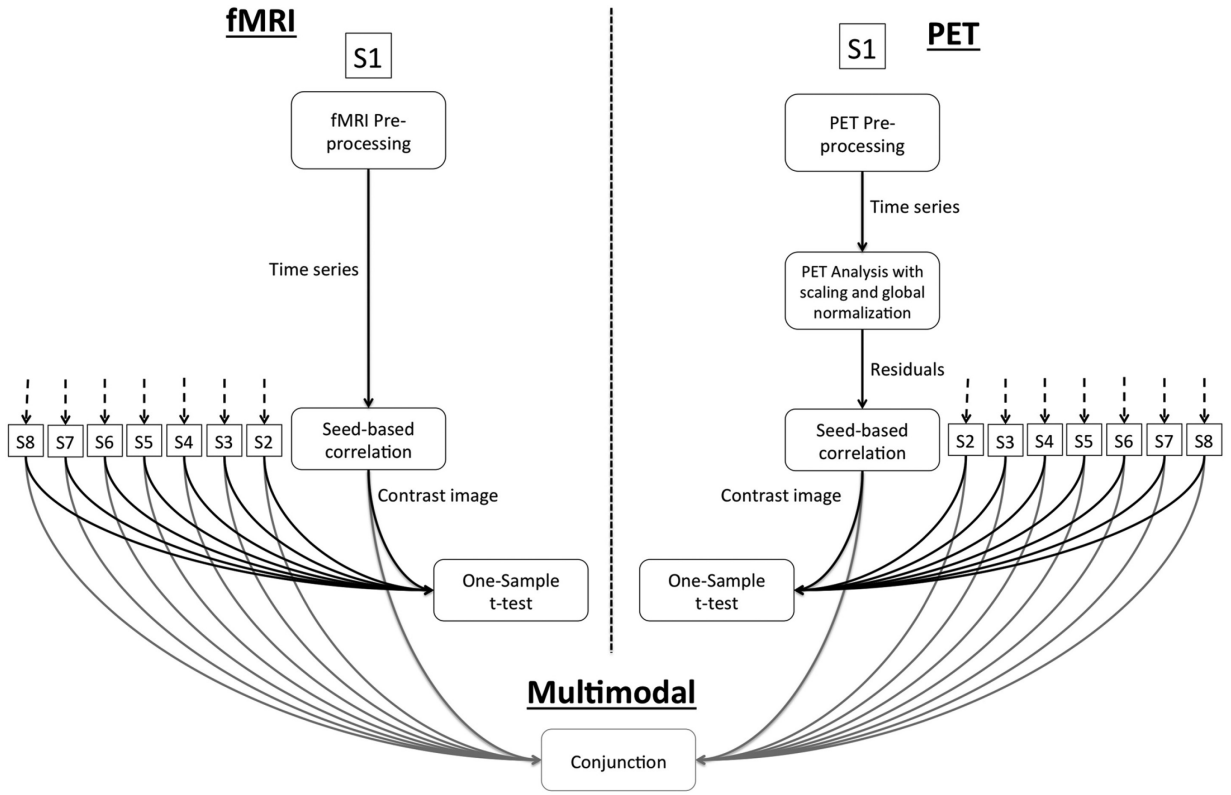

Figure 2.
Graphical illustration of seed-based correlation analysis of fMRI and PET data and conjunction analysis.

The statistical analysis of the PET data was specifically developed for this study, since the analysis of temporal–spatial correlation of resting-state PET is, up to now, a nonstandard approach for PET data. The analysis consisted of three consecutive analyses (see Fig. 2). The first two analyses were performed on the single-subject level and only the third analysis was conducted as a group analysis. The first analysis was a standard PET analysis with the exception that the residuals of this analysis were kept and used as input for the second analysis. This first analysis rested on a general linear model that assumed a constant global blood flow and accounted for global variations in the total intensity of the PET images, caused by the different number of counts between the images. Thus, the FDG-PET time series was scaled to represent a constant global blood flow of 50 ml/100 g/min and subjected to a one-sample *t*-test. To account for the increasing intensity due to inflow and uptake of the radioactive FDG, a global normalization was performed by including the global intensity of each time frame as additional covariate. The analysis was restricted to voxels with an intensity of at least 80% of the global mean.

Through the use of a slightly modified version of SPM8, the residuals of this design were kept after the model had been fitted. The resulting twelve residual images, representing the local fluctuation in the FDG-uptake for each voxel, were subjected to the second single-subject analysis, that is, the seed-based correlation analysis. Comparable to the fMRI seed-based correlation analysis, local fluctuations in the FDG-uptake from the dorsal dPCC were included by extracting the intensity values within the dPCC from these residual images. These values were included as a covariate but without any scaling or global normalization. Finally, the individual beta-weights from these seed-based correlation analyses were subjected to the third analysis, which was a one-sample *t*-test across all eight participants, with age as an additional covariate. Since both directions of the correlation were tested, the results from this analysis were explored with a corrected significance threshold of $P < 0.025$, corrected for multiple comparisons, using FDR correction, and at least 50 voxels per cluster.

Joint fMRI and PET Data Analysis

As can be seen in Figure 2, for a joint analysis of the fMRI and PET-data, the respective beta-weights of both, the fMRI and PET seed-based correlation analysis, were also combined in an ANOVA model,

corrected for age, and a conjunction across modalities was estimated and explored with a significance threshold of $P < 0.025$ (FDR-corrected) and with at least 50 voxels per cluster.

In addition to these voxel-wise analyses, a joint analysis was performed by investigating whether the local fluctuation in glucose consumption is associated with functional connectivity within the DMN. Therefore, mean FDG-uptake for the MdFG, PCC, right and left ANG reflecting the main nodes of the DMN, were computed. The same ROIs as for the time series extraction (see Resting-state fMRI analysis) were used. The individual cross-correlation coefficients, reflecting individual DMN within-network connectivity, were *z*-transformed and correlated with individual mean FDG-uptake values of the respective DMN-node. To investigate whether glutamatergic neurotransmission influences within-network connectivity, the same correlation analysis was done with individual Glx concentration values (for further details see ^{1}H-MRS analysis) from the precuneus. Given the small number of participants Spearman's rank-order correlation were used. All correlation were controlled for the participants' age and the significance threshold was set to $P < 0.05$. The *P*-value was not corrected for multiple comparisons to preserve statistical power.

^{1}H-MRS Analysis

Analysis of ^{1}H-MRS spectra was performed in LCModel version 6.3-1B [Provencher, 1993], using a simulated basis set of 15 metabolites, that is, L-alanine, aspartate, creatine, GABA, glucose, glutamine, glutamate, glycerophosphocholine, phosphocholine, L-lactate, myo-inositol, *N*-acetyl aspartate, *N*-acetyl aspartate glutamate, scyllo-inositol, and taurine. Metabolite estimates were scaled to a water reference, and adjusted for local water density to account for partial volume effects. Water concentration within the voxel (i.e., left precuneus) was estimated by segmenting the T1-weighted structural image into gray matter (GM), white matter, and cerebral spinal fluid components. Combined segmentation and spatial normalization functions of SPM8, applying standard literature values of density for each tissue class and integrating across the voxel after coregistering with the T2 image on which the voxel had been initially positioned, were used.

Values for Glx, denoting the sum of the estimates for glutamate and glutamine components, were used in this analysis, as it reflects the glutamatergic pool available for synaptic-metabolic activity [Yüksel and Öngür, 2010], and can be considered as an adequate representation of glutamatergic neurotransmission. The Cramér-Rao Lower Bound (CRLB) for Glx was lower 20%; additional qualitative checks were also performed, both visually and using in-house algorithms to identify aberrant spectra (i.e., spurious peaks, artifacts, any apparent errors in the fitting process). As the concentration of glutatmate has been shown to depend on the GM volume within the measured region of interest [Srinivasan et al., 2006], Glx concentrations were residualized for the proportion of GM within the area of the brain bounded by the MRS-voxel. More specifically, we did a linear regression analysis to study the association between individual Glx concentrations and individual GM volumes and saved the standardized residuals for further statistical analyzes.

RESULTS

Seed-Based Correlation and Conjunction Analysis

The seed-based correlation analysis of fluctuations of FDG-uptake within the dPCC revealed a widespread and mostly symmetrical network of areas showing a positive correlation. Besides a strong correlation within the dPCC, positive correlations were found for the precuneus, the left and right inferior parietal lobe (IPL), extending into the left ANG, the superior part of the middle frontal gyrus (MFG) of both hemispheres, medial frontal gyrus (MdFG), the supplementary motor area (SMA), and the left inferior frontal gyrus (IFG; see Table II and Fig. 3a). In addition, positive correlations were seen for the left and right putamen and the occipital lobe. Negative correlations were detected only for the right parahippocampal gyrus, extending into the temporal pole (see Table II and Fig. 3d).

Similarly, the seed-based correlation analysis for the fMRI data revealed strong correlation within the dPCC and precuneus, as well as bilaterally ANG, IPL, MdFG, MFG, and IFG. In addition, positive correlations were seen for the SMA, left superior temporal gyrus, right caudate nucleus, right lingual gyrus, and the rostral part of the anterior cingulate cortex (see Table II and Fig. 3b). No negative correlations were detected.

The conjunction analyses demonstrated a high level of similarity between both modalities, in particular for the PCC, precuneus, left and right ANG and IPL, left and right MFG, the SMA and MdFG, as well as for the superior occipital gyrus (see Table II and Fig. 3c).

Independent Component and Correlation Analysis

The temporal concatenation ICA revealed eight ICs that were in correspondence with commonly identified RSNs (e.g., van den Heuvel and Pol, 2010]. Spatial maps of the ICs can be found in Supporting Information Figure 1. The IC4, including the MdFG, PCC, right, and left ANG, was taken as a representative component for the DMN. The spatial pattern of the DMN and the within-network connectivity matrices are shown in Figure 4. Not surprisingly, within-network connectivity analyses showed significant positive correlations ($P < 0.0001$) between all DMN network nodes.

Spearman's rank correlation analyses between individual within-network coupling and mean FDG-uptake showed a significant positive correlation between glucose

TABLE II. Results of seed-based (dorsal posterior cingulate cortex) correlation and conjunction analysis: anatomical localizations, MNI coordinates and significance values of the peak voxel. Results are false-discovery rate (FDR)-corrected, $k > 50$ voxel.

Region	MNI coordinates			*P*-value	*t*-value	*z*-value	Cluster size (#voxel)
	x	*y*	*z*				
PET: Positive correlation [p(FDR) < 0.025]							
PCC, Precuneus	4	−22	38	0.000	77.36	6.29	2182
MdFG, MFG, SMA	6	26	62	0.000	25.11	5.15	1943
MFG, IFG	−48	22	38	0.001	21.22	4.96	616
Putamen	−18	10	0	0.002	15.90	4.62	94
ANG, IPL	−42	−54	40	0.002	14.91	4.54	164
Calcarine	0	−94	4	0.003	14.51	4.50	113
Putamen	36	2	0	0.004	13.25	4.39	235
Paracentral	−14	−26	62	0.005	11.51	4.21	72
MFG	40	52	6	0.007	10.40	4.07	94
Calcarine	4	−60	10	0.014	7.70	3.66	168
PET: Negative correlation [p(FDR) < 0.025]							
Temporal Pole, Parahippocampal Gyrus	24	−4	−34	0.012	21.80	4.99	149
fMRI: Positive correlation [p(FDR) < 0.001]							
PCC, Precuneus	−10	−56	48	0.000	36.83	5.56	1787
MFG (L & R), SMA, MdFG, MCC, ACC	26	60	6	0.000	31.12	5.38	4716
ANG, SMG, STG	−52	−50	34	0.000	27.07	5.23	320
Caudate Nucleus	24	6	22	0.001	15.71	4.60	221
Lingual Gyrus	10	−44	2	0.001	14.91	4.54	129
Precentral Gyrus	−32	−4	64	0.001	14.78	4.53	124
rostral ACC	−10	50	0	0.001	13.95	4.45	60
IPL, ANG	50	−52	46	0.001	13.59	4.42	148
PET & fMRI conjunction: Positive correlation [p(FDR) < 0.025]							
MFG (L&R), SMA	−30	26	42	0.002	10.93	5.27	4624
PCC, Precuneus	−6	−20	42	0.002	10.10	5.11	5793
MdFG	2	46	28	0.002	8.92	4.85	214
IPL, ANG	−42	−52	40	0.002	8.24	4.69	604
MFG	38	52	8	0.002	7.10	4.37	214
IPL, ANG	36	−46	44	0.004	5.67	3.88	390
SOG	−20	−88	36	0.008	4.77	3.51	72
Precuneus	−12	−36	58	0.010	4.46	3.36	57

consumption in PCC and lANG and the coupling between PCC and lANG, [$r_s(5) = 0.95$; $P < 0.05$] and [$r_s(5) = 0.78$; $P < 0.05$], respectively. Further, glucose consumption in MFG correlated positively with functional connectivity between the lANG and rANG [$r_s(5) = 0.85$; $P < 0.05$]. All other correlations failed to be significant (all ps > 0.05). Thus, higher FDG-uptake in MdFG PCC, and lANG predicted the functional coupling between specific DMN network nodes.

The correlation coefficients between within-network coupling and Glx concentration in the precuneus were not significant.

DISCUSSION

Using a multimodal approach, we found substantial similarities in the spatial patterns of fluctuations in FDG-uptake and fluctuations in the BOLD signal, when taking the dorsal posterior cingulate cortex as seed region. Signals in the DMN brain areas, comprising the inferior parietal lobe, angular gyrus, precuneus, middle, and medial frontal gyrus, were strongly correlated with signals in the dorsal posterior cingulate cortex during rest, for both modalities. Furthermore, we found significant positive correlations between FDG-uptake in the medial frontal gyrus, posterior cingulate cortex, and left angular gyrus and functional connectivity between specific DMN nodes. This reflects that local glucose consumption is related to DMN within-network functional connectivity. No significant relationship was found between glutamatergic neurotransmission, measured by ^{1}H-MRS, and functional connectivity.

Similarities and Differences between fMRI and FDG-PET Correlation Maps

The results of the seed-based correlation analysis demonstrated a quite remarkable spatial overlap between fMRI

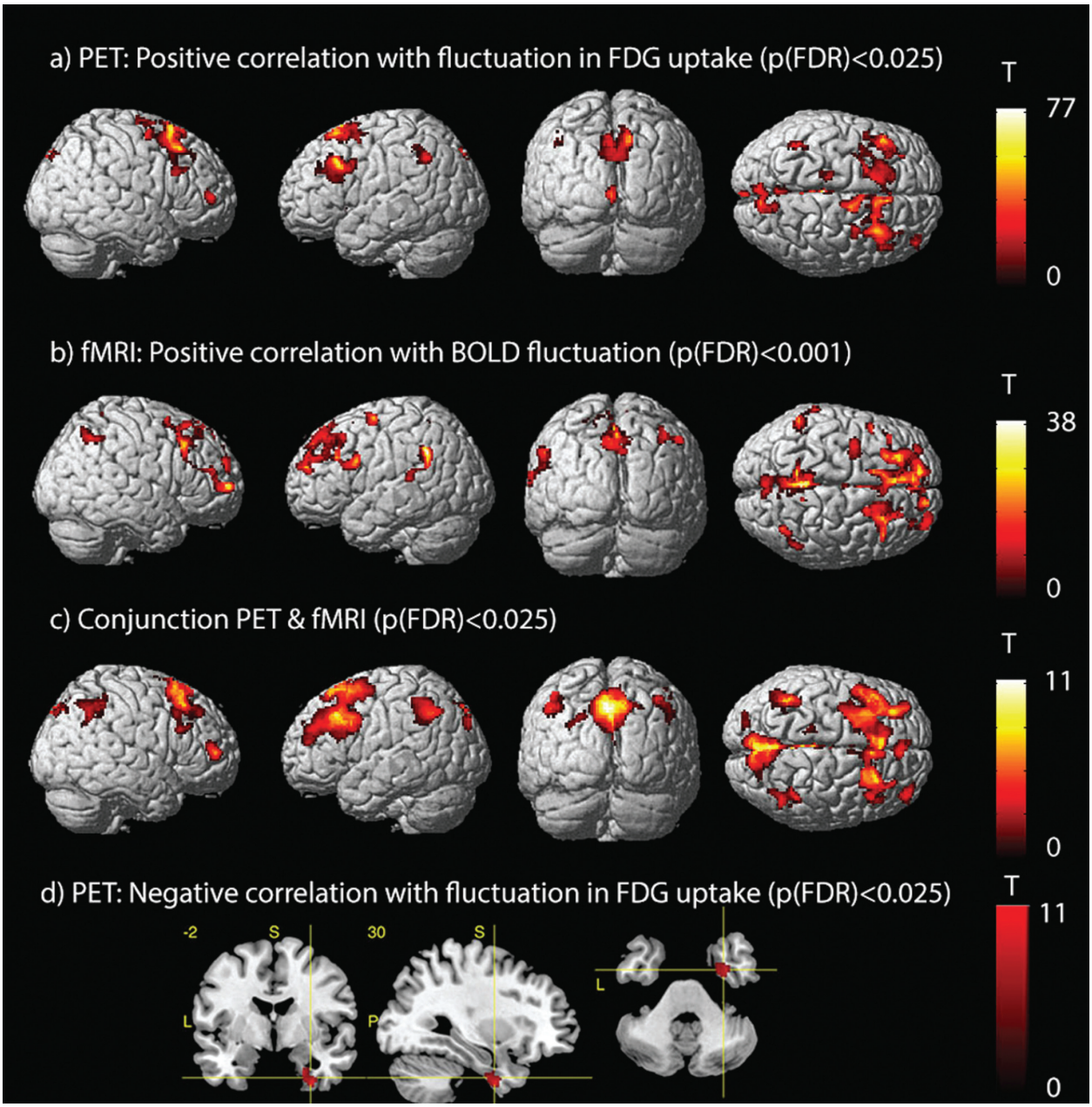

Figure 3.

Spatial maps for seed-based correlations, with the dorsal posterior cingulate cortex as seed region. (**A–C**) Spatial maps display positive correlation with fluctuations within the seed region for (A) FDG-uptake, measured with PET, (B) BOLD signal, measured with resting-state fMRI, (C) Conjunction of the two modalities, and (**D**) Negative correlation for FDG-uptake. All results are displayed with corrected thresholds, as indicated in the figure, with at least 50 voxels per cluster.

and FDG-PET data. More specifically, the results of the conjunction analysis showed that in both modalities the same areas in the inferior parietal lobe, angular gyrus, precuneus, middle, and medial frontal gyrus were positively correlated to the dorsal posterior cingulate cortex. These findings suggest that the functionally related brain regions reflected by fMRI also have similar variance in glucose metabolism, a direct indicator of neuronal activity. Thus, the correlation of spontaneous fluctuations in BOLD signals in these regions likely originates from dynamic changes in local neuronal activity [Riedl et al., 2014; Tomasi et al., 2013; Wu et al., 2009].

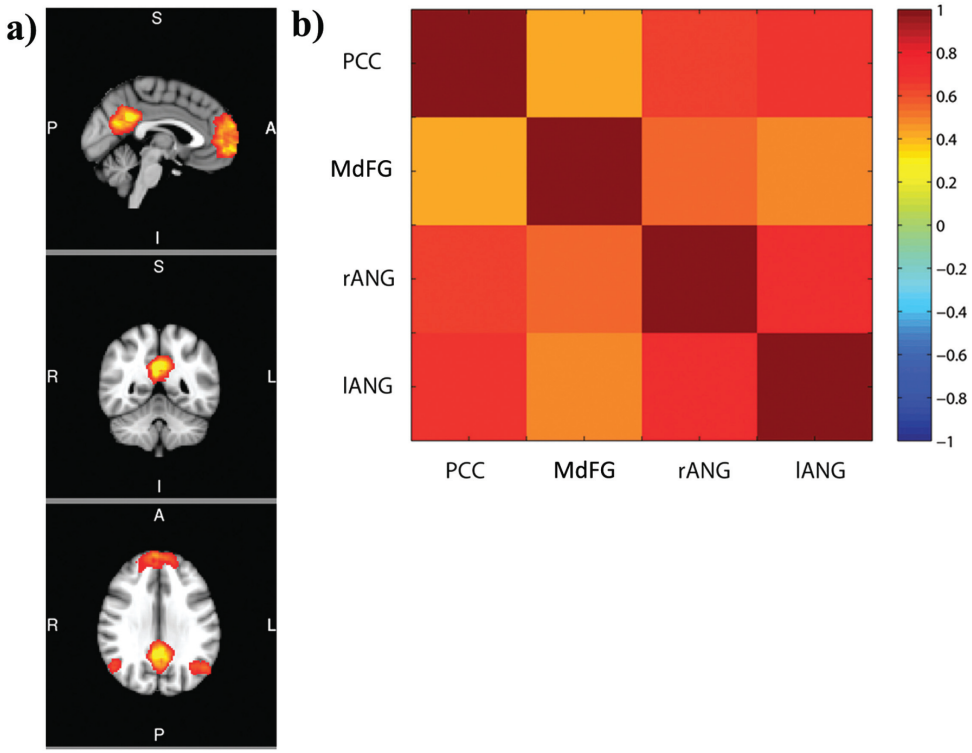

Figure 4.

Spatial map and functional connectivity of default-mode network (DMN). (**A**) Group spatial map of DMN including posterior cingulate cortex (PCC), medial frontal gyrus (MdFG), right angular gyrus (rANG), and left angular gyrus (lANG) is shown using a z-score > 4 threshold and in radiological orientation (A = anterior, I = inferior, L = left, P = posterior, R = right, S = superior). (**B**) Within-network connectivity matrices for the DMN. Vertical and horizontal partitions reflect the four DMN nodes. All correlations were significantly positive, $P < 0.0001$.

Interestingly, negative correlations were found for the PET data within the right parahippocampal gyrus and temporal pole. Although the dorsal posterior cingulate cortex is strongly interconnected with the limbic system, direct negative correlations between DMN-related areas and the parahippocampal gyrus have not yet been reported. In contrast, no negative associations were observed for the fMRI data.

In general, it should be kept in mind that the fluctuations in FDG-uptake and the corresponding fluctuations in the BOLD signal were measured in different temporal scales. While the fMRI dataset has a temporal resolution of 1.5 s and in total 300 images, the measurement of fluctuations in FDG-uptake is based on twelve time frames, representing continuous FDG-uptake over 5 min. Thus, it is not surprising that the spatial pattern is divergent in some brain areas. Furthermore, the acquisition of PET resting-state data took place in a relatively silent environment, while fMRI-based resting-state data acquisitions are always accompanied by intense scanner noise. This might explain the additional activation in the superior temporal gyrus, present in the fMRI [e.g., Binder et al., 2000; Rimol et al., 2005; Wong et al., 2008] but not in the FDG-PET data.

Taken together, there is a striking overall similarity across the two modalities with respect to positive correlations, despite the latter being measured on a different, low resolution time scale. In line with previous rs-fMRI research, this might indicate that resting-state BOLD fluctuations actually derive from low-frequency spontaneous events [Gaudes et al., 2011; Liu and Duyn, 2013]. However, due to the different temporal scales, it is not possible to infer whether there is a temporal relationship between the fluctuations of FDG-uptake and fluctuations in the BOLD signal. To investigate the temporal relationship further, future studies using the same experiment should take advantage of simultaneous PET/fMRI scanning and new PET-FDG approaches (fPET-FDG) in which FDG delivery is controlled by constant infusion to track changes in FDG metabolism in a more dynamic mode and with higher temporal resolution [Villien et al., 2014].

Association between Local Glucose Metabolism and within-Network Connectivity

Mean FDG-uptake in the medial frontal gyrus, posterior cingulate cortex, and left angular gyrus correlated

significantly with the functional connectivity between specific DMN nodes. More specifically, increased glucose consumption in the medial frontal gyrus was associated with an increase in functional coupling between the right and left angular gyrus. Similarly, increased glucose consumption in the posterior cingulate cortex and left angular gyrus was linked to an increased coupling between these two nodes. These associations are in line with findings from recent FDG-PET/fMRI-studies which provide evidence for a close interaction between local glucose consumption and functional connectivity derived from BOLD fMRI [Riedl et al., 2014; Tomasi et al., 2013].

In contrast to previous findings that have shown a positive association between resting-state glutamate level and DMN functional connectivity [Enzi et al., 2012; Hu et al., 2013], we did not reveal any significant association between local glutamatergic neurotransmission, here measured in the left precuneus, and DMN functional connectivity. For instance, Enzi et al., [2012] showed in a group of nineteen healthy subjects that increased glutamate concentration in the perigenual anterior cingulate cortex, also a part of the DMN, is associated with higher DMN activity during rest. In addition, Hu et al., [2013] examined a group of twenty-four healthy subjects and found that high glutamate concentration in the posterior cingulate cortex was associated with reduced deactivation of the DMN probed by a working memory task. These findings suggest that glutamatergic neurotransmission measured in subnodes of the DMN has an effect on DMN functional connectivity and its task-dependent down-regulation. The absence of a significant association in the present study may be explained by the differences in voxel placement and/or the small sample size in our study. Future studies with larger sample size should systematically examine whether the association between glutamatergic neurotransmission and functional connectivity varies across subregions of the DMN.

Limitations

As has been mentioned before, a major limitation to our study is the small sample size. Thus, the association between local glucose consumption and functional connectivity reported here, needs to be replicated in an independent sample before drawing strong conclusions. The present study examines only one aspect of the physiological complexity that the BOLD signal is based on. Thus, future studies should, additionally consider [^{15}O]water PET and/or arterial spin labeling to quantify cerebral blood flow [Zhang et al., 2014] and respiratory-based BOLD calibration methods to measure within-subject changes in absolute $CMRO_2$ across the brain [Wise et al., 2013]. Furthermore, it should be investigated whether the association between local glucose consumption, glutamatergic neurotransmission, and DMN functional connectivity varies between rest and an attention-demanding task condition. Ideally, the modalities should be assessed simultaneously or at least in close temporal proximity by taking advantage of an integrated PET/MR scanner. FDG metabolism should be assessed in a more dynamic mode with higher temporal resolution using fPET-FDG approaches [Villien et al., 2014] to investigate the temporal correlation between FDG and BOLD fluctuations. This may shed new light on the exact mechanisms of the down-regulation of the DMN during attention and cognitive control processes, and provide novel insights towards a better understanding of aberrant DMN deactivation in psychiatric patients (see Whitfield-Gabrieli and Ford, 2012 for overview).

CONCLUSION

The present study showed clear spatial similarities between fluctuations in local glucose consumption and fluctuations in BOLD signal. Furthermore, we revealed that local glucose consumption was positively correlated with functional connectivity within the DMN reflecting a close interaction between the two modalities. In accordance with very recent findings, these results further support that BOLD signal fluctuations, and thus functional connectivity during rest, likely derive from dynamic changes in cerebral metabolism reflecting ongoing neuronal activity. Future studies with larger samples should investigate the temporal aspects of this interaction and whether this association changes between rest and an attention-demanding condition to gain more insights into the metabolic origin of the task-dependent down regulation of the DMN.

ACKNOWLEDGMENTS

The authors thank all radiographers at the Department of Radiology at Haukeland University Hospital, Bergen, Norway, for their support in data acquisition. Further thanks go to the head of the Department of Radiology, Haukeland University Hospital, Aslak Aslaksen, for providing the necessary infrastructure.

REFERENCES

Ai-Ling L, Fox PT, Yihong Y, Hanzhang L, Li-Hai T, Jia-Hong G (2008): Evaluation of MRI models in the measurement of CMRO 2 and its relationship with CBF. Magn Reson Med 60: 380–389.

Beckmann CF, DeLuca M, Devlin JT, Smith SM (2005): Investigations into resting-state connectivity using independent component analysis. Philos Trans R Soc B Biol Sci 360:1001–1013.

Binder JR, Frost JA, Hammeke TA, Bellgowan PS F., Springer JA, Kaufman JN, Possing ET (2000): Human temporal lobe activation by speech and nonspeech sounds. Cereb Cortex 10:512–528.

Biswal B, Yetkin FZ, Haughton VM, Hyde JS (1995): Functional connectivity in the mototr cortex of resting human brain using echo-planar MRI. Magn Reson Med 34:537–541.

Bonvento G, Sibson N, Pellerin L (2002): Does glutamate image your thoughts? Trends Neurosci 25:359–364.

Brookes MJ, Woolrich M, Luckhoo H, Price D, Hale JR, Stephenson MC, Barnes GR, Smith SM, Morris PG (2011): Investigating the electrophysiological basis of resting state networks using magnetoencephalography. Proc Natl Acad Sci USA 108:16783–16788.

Buxton RB, Wong EC, Frank LR (1998): Dynamics of blood flow and oxygenation changes during brain activation: The balloon model. Magn Reson Med 39:855–864.

Damoiseaux JS, Rombouts S, Barkhof F, Scheltens P, Stam CJ, Smith SM, Beckmann CF (2006): Consistent resting-state networks across healthy subjects. Proc Natl Acad Sci USA 103: 13848–13853.

Di X, Biswal BB, Alzheimer's Disease Neuroimaging Initiative (2012): Metabolic brain covariant networks as revealed by FDG-PET with reference to resting-state fMRI networks. Brain Connect 2:275–283.

Enzi B, Duncan NW, Kaufmann J, Tempelmann C, Wiebking C, Northoff G (2012): Glutamate modulates resting state activity in the perigenual anterior cingulate cortex—A combined fMRI-MRS study. Neuroscience 227:102–109.

Falkenberg LE, Westerhausen R, Specht K, Hugdahl K (2012): Resting-state glutamate level in the anterior cingulate predicts blood-oxygen level-dependent response to cognitive control. Proc Natl Acad Sci USA 109:5069–5073.

Fox MD, Raichle ME (2007): Spontaneous fluctuations in brain activity observed with functional magnetic resonance imaging. Nat Rev Neurosci 8:700–711.

Fox MD, Snyder AZ, Vincent JL, Corbetta M, Van Essen DC, Raichle ME (2005): The human brain is intrinsically organized into dynamic, anticorrelated functional networks. Proc Natl Acad Sci USA 102:9673–9678.

Gaudes CC, Petridou N, Dryden IL, Bai L, Francis ST, Gowland PA (2011): Detection and characterization of single-trial fMRI BOLD responses: Paradigm free mapping. Hum Brain Mapp 32:1400–1418.

Greicius MD, Krasnow B, Reiss AL, Menon V (2003): Functional connectivity in the resting brain: A network analysis of the default mode hypothesis. Proc Natl Acad Sci USA 100:253–258.

Heeger DJ, Ress D (2002): What does fMRI tell us about neuronal activity? Nat Rev Neurosci 3:142–151.

Hu YZ, Chen X, Gu H, Yang YH (2013): Resting-state glutamate and GABA concentrations predict task-induced deactivation in the default mode network. J Neurosci 33:18566–18573.

Jenkinson M, Bannister P, Brady M, Smith S (2002): Improved optimization for the robust and accurate linear registration and motion correction of brain images. Neuroimage 17:825–841.

Lauritzen M (2005): Reading vascular changes in brain imaging: is dendritic calcium the key? Nat Rev Neurosci 6:77–85.

Leech R, Kamourieh S, Beckmann CF, Sharp DJ (2011): Fractionating the default mode network: Distinct contributions of the ventral and dorsal posterior cingulate cortex to cognitive control. J Neurosci 31:3217–3224.

Liu X, Duyn JH (2013): Time-varying functional network information extracted from brief instances of spontaneous brain activity. Proc Natl Acad Sci USA 110:4392–4397.

Logothetis NK, Wandell BA (2004): Interpreting the BOLD signal. Annu Rev Physiol 66:735–769.

Provencher SW (1993): Estimation of metabolite concentrations from localized in-vivo proton NMR-spectra. Magn Reson Med 30:672–679.

Raichle ME (1987): Circulatory and metabolic correlates of brain function in normal humans. In: Mountcastle MB, Plum F, Geiger, SR, editors. Handbook of Physiology—The Nervous System. Bethesda: American Physiological Society. pp 643–674.

Raichle ME, MacLeod AM, Snyder AZ, Powers WJ, Gusnard DA, Shulman GL (2001): A default mode of brain function. Proc Natl Acad Sci USA 98:676–682.

Raichle ME (2010): Two views of brain function. Trends Cognit Sci 14:180–190.

Riedl V, Bienkowska K, Strobel C, Tahmasian M, Grimmer T, Forster S, Friston KJ, Sorg C, Drzezga A (2014): Local activity determines functional connectivity in the resting human brain: A simultaneous FDG-PET/fMRI study. J Neurosci 34:6260–6266.

Rimol LM, Specht K, Weis S, Savoy R, Hugdahl K (2005): Processing of sub-syllabic speech units in the posterior temporal lobe: An fMRI study. Neuroimage 26:1059–1067.

Rytty R, Nikkinen J, Paavola L, Abou Elseoud A, Moilanen V, Visuri A, Tervonen O, Renton, A.E., Traynor, B.J., Kiviniemi V, Remes AM (2013): GroupICA dual regression analysis of resting state networks in a behavioral variant of frontotemporal dementia. Front Hum Neurosci 7:461.

Sala-Llonch R, Pena-Gomez C, Arenaza-Urquijo EM, Vidal-Pineiro D, Bargallo N, Junque C, Bartres-Faz D (2012): Brain connectivity during resting state and subsequent working memory task predicts behavioural performance. Cortex 48:1187–1196.

Shulman RG, Hyder F, Rothman DL (2001): Cerebral energetics anti the glycogen shunt: Neurochemical basis of functional imaging. Proc Natl Acad Sci USA 98:6417–6422.

Smith SM (2002): Fast robust automated brain extraction. Hum Brain Mapp 17:143–155.

Srinivasan R, Cunningham C, Chen A, Vigneron D, Hurd R, Nelson S, Pelletier D (2006) TE-averaged two-dimensional proton spectroscopic imaging of glutamate at 3 T. Neuroimage 30: 1171–1178.

Tomasi D, Wang GJ, Volkow ND (2013): Energetic cost of brain functional connectivity. Proc Natl Acad Sci USA 110:13642–13647.

Tzoulis C, Tran GT, Schwarzlmuller T, Specht K, Haugarvoll K, Balafkan N, Lilleng PK, Miletic H, Biermann M, Bindoff LA (2013): Severe nigrostriatal degeneration without clinical parkinsonism in patients with polymerase gamma mutations. Brain 136:2393–2404.

van den Heuvel MP, Pol HEH (2010): Exploring the brain network: A review on resting-state fMRI functional connectivity. Eur Neuropsychopharmacol 20:519–534.

Villien M, Wey, H.-Y., Mandeville JB, Catana C, Polimeni JR, Sander CY, Zürcher NR, Chonde DB, Fowler JS, Rosen BR, Hooker JM (2014): Dynamic functional imaging of brain glucose utilization using fPET-FDG. Neuroimage 100:192–199.

Vincent JL, Patel GH, Fox MD, Snyder AZ, Baker JT, Van Essen DC, Zempel JM, Snyder LH, Corbetta M, Raichle ME (2007): Intrinsic functional architecture in the anaesthetized monkey brain. Nature 447:83–86.

Wehrl HF, Hossain M, Lankes K, Liu CC, Bezrukov I, Martirosian P, Schickt F, Reischl G, Pichler BJ (2013): Simultaneous PET-MRI reveals brain function in activated and resting state on metabolic, hemodynamic and multiple temporal scales. Nat Med 19:1184–1189.

Wise RG, Harris AA, Stone AJ, Murphy K (2013): Measurement of OEF and absolute CMRO2: MRI-based methods using interleaved and combined hypercapnia and hyperoxia. Neuroimage 83:135–147.

Whitfield-Gabrieli S, Ford JM (2012): Default mode network activity and connectivity in psychopathology. Annu Rev Clin Psychol 8:49–76.

Wong PC M., Uppunda AK, Parrish TB, Dhar S (2008): Cortical mechanisms of speech perception in noise. J Speech Lang Hearing Res 51:1026–1041.

Wu CW, Gu H, Lu HB, Stein EA, Chen JH, Yang YH (2009): Mapping functional connectivity based on synchronized CMRO2 fluctuations during the resting state. Neuroimage 45: 694–701.

Yüksel C, Öngür D (2010): Magnetic resonance spectroscopy studies of glutamate-related abnormalities in mood disorders. Biol Psychiatry 68:785–794.

Zhang K, Herzog H, Mauler J., Filss C, Okell TW, Kops ER, Tellmann L1, Fischer T3, Brocke B3, Sturm W4, Coenen HH, Shah NJ (2014). Comparison of cerebral blood flow acquired by simultaneous [15O]water positron emission tomography and arterial spin labeling magnetic resonance imaging. J Cerebral Blood Flow Metab 34:1373–1380.